Title

Low Voltage, High Optical Power Handling Capable, Bulk Compound Semiconductor Electro-Optic Modulators at 1550 nm

Journal

Journal of Lightwave Technology, 38(8)

ISSN

0733-8724

Authors

Bhasker, Prashanth
Norman, Justin
Bowers, John
et al.

Publication Date

2020

DOI

10.1109/jlt.2020.2964618

Peer reviewed

Low Voltage, High Optical Power Handling Capable, Bulk Compound Semiconductor Electro-optic Modulators at 1550 nm

Prashanth Bhasker, Justin Norman, John Bowers, *Fellow, IEEE* and Nadir Dagli, *Fellow, IEEE*

***Abstract*— AlGaAs bulk electro-optic Mach-Zehnder modulators with low V_π are reported. Epilayer design is an *npin*, which is shown to be equivalent to a *pin*. Measured V_π is 1 V for 1 cm long electrode and this result agrees very well with numerical modeling. Modulator capacitance remains constant and current through the device is negligible over a wide bias range. Lowest bandgap of the material in the active waveguide region is larger than twice the photon energy at 1550 nm significantly reducing material absorption, including two-photon absorption. Modulator characteristics remain unchanged under coupled input optical powers approaching 160 mW. Low V_π combined with high optical power handling capability make these devices suitable for analog photonic links.**

***Index Terms*— Compound semiconductors, optical modulation, optical waveguides, phase modulation.**

I. Introduction

Optical systems ranging from fiber optic communication to on chip optical interconnects usually require an optical modulator to bring electrical signals to optical domain. Hence, an optical modulator is an essential component to realize optical systems. Certain modulator requirements are common to all applications. Some applications require specific modulator features, such as high degree of linearity or high extinction ratio. Analog photonic links that enable transmission of wideband analog electrical signals to distant destinations over the optical fiber is one such example. Such links can provide wide 3 dB electrical bandwidths, low weight, low cost and gain provided that appropriate modulators are available. The gain of an analog link is proportional to P/V_π, where P is the maximum optical output power of the modulator and V_π is the voltage required to switch a Mach-Zehnder modulator (MZM) from on to off state or vice versa. [1]. Therefore, a low V_π modulator that can handle large optical power is very desirable. There are various technologies to realize such modulators [2], [3]. Most mature modulator technology is based on $LiNbO_3$. However, such modulators have high V_π and large size [2]. Low voltage modulators have been realized in other material systems. For example, carrier injection silicon Mach Zehnder modulators can have V_π as low as 1.8 V [4] but suffer from low bandwidth. Slow wave designs have also been used to provide about 1 V V_π over very limited optical bandwidth [5]. Polymer modulators offer very wide bandwidth but have large V_π and degradation issues at high optical powers [6]. Our recent work using compound semiconductor substrate removed waveguides resulted in 0.2 V V_π Mach Zehnder intensity modulators [7]. Using a different substrate removed waveguide, we also demonstrated 0.77 V V_π and bandwidth exceeding 67 GHz at 1550 nm [8]. The modulator should also be able to transmit high optical powers in addition to having a low V_π. This requires very low material absorption, in addition to low optical propagation and coupling loss. In compound semiconductors, low coupling loss is achieved using mode transformers. Low propagation loss is also possible through careful lithography, processing and doping design. However, these very low V_π devices used $In_{0.52}Al_{0.48}As$/ $In_{0.53}Ga_{0.39}Al_{0.08}As$ multi quantum well (MQW) cores on InP for improved electro-optic efficiency for V_π reduction. MQW cores start to absorb under high electric fields and limit the optical power handling of these devices. In principle, material absorption can be eliminated using materials with bandgap larger than the photon energy. However, at high power levels two-photon absorption emerges as another source of absorption [9]. This can be dealt by using material with bandgap larger than twice the photon energy. This requires a minimum bandgap of 1.6 eV at 1.55 μm and severely limits the material choice. In III-V compound semiconductors, GaAs/AlGaAs material system is a suitable candidate for high optical power applications. This material system is transparent at 1.55 μm, provides large bandgap adjustment and index differences around 0.45. Such large index steps enable compact waveguides, which is essential to reduce the V_π. In addition,

Manuscript received xxx xx, 2019; revised xxx x, 2019; accepted xxx xx, 2019. This work was supported in part by the Air Force Research Laboratory under FA8650-15-2-5220 and in part by an NSF Grant 1711446. *(Corresponding author: Nadir Dagli.)*

P. Bhasker and N. Dagli are with the Electrical and Computer Engineering Department, University of California Santa Barbara, Santa Barbara, CA 93016 USA (e-mail: prashanth@umail.ucsb.edu; dagli@ucsb.edu).

J. Norman is with the Materials Department, University of California Santa Barbara, Santa Barbara, CA 93016 USA (e-mail: jcnorman223@gmail.com).

J. Bowers is with the Materials and Electrical and Computer Engineering Departments, University of California Santa Barbara, Santa Barbara, CA 93016 USA (e-mail: bowers@ece.ucsb.edu)

advanced processing techniques allow the fabrication of novel geometries with very low V_π. For example, bonding and substrate removal enable very uniform sub-micron electrode gaps and resulted in the fabrication of bulk GaAs modulators with V_π as low as 0.3 V [10]. However, bonding and substrate removal are not among the conventional foundry techniques at the moment. This makes low V_π wide bandwidth modulators fabricated on growth substrates using conventional foundry processes highly desirable.

In this paper, a GaAs/AlGaAs based electro optic modulator operating at 1.55 μm with a low V_π of 1 V is demonstrated. The lowest material bandgap used in the device is more than twice the photon energy. As a result, the modulator can handle very high optical powers with negligible material absorption. Fabrication requires conventional processing methods and the device can be made very wide bandwidth using previously demonstrated electrode designs [11]. Preliminary results of this work were reported in [12]. In this paper, we present further data on design details, IV and CV characteristics, details of fabrication, operation under high optical powers as well as a detailed discussion of the data. Next section addresses device description and design followed by processing details. Experimental results are then presented and discussed. Finally, conclusions are given.

II. Device Description and Design

Epitaxial layers were grown by molecular beam epitaxy (MBE) at 600ºC on a [100] semi-insulating (SI) GaAs substrate. Before growing the device layers, two pairs of alternating layers of 0.2 μm thick GaAs and 0.2 μm thick AlAs were grown as etch stop layers. These layers do not contribute to the operation of the device but allow the removal of the growth substrate if desired. Following that, 0.1 μm thick $n^+ \approx 10^{18}$ cm^{-3} GaAs, 1.2 μm thick $n = 1\times10^{17}$ cm^{-3} $Al_{0.9}Ga_{0.1}As$, unintentionally doped (UID) 0.25 μm thick $Al_{0.2}Ga_{0.8}As$, UID 0.02 μm $Al_{0.9}Ga_{0.1}As$, 0.1 μm thick $p = 4\times10^{17}$ cm^{-3} $Al_{0.2}Ga_{0.8}As$, 1.2 μm thick $n = 1\times10^{17}$ cm^{-3} $Al_{0.9}Ga_{0.1}As$, and 0.1 μm thick $n^+ \approx 10^{18}$ cm^{-3} GaAs were grown as the device layers. *n* and *p* dopants were silicon and beryllium respectively. This *npin* device is electrically equivalent to two back-to-back diodes connected in series as shown in Fig. 1. This design is preferable to the regular *pin* design since there is no ohmic contact to the *p* layer. Hence, microwave loss due to high resistance *p* contacts are eliminated. However, there is increased optical and electrical loss due to the presence of the *p* layer in the waveguide. But, under regular operation most of the *p* layer is depleted and the overlap of this layer with the optical and microwave modes are very low, making this loss tolerable. Under bias between the n^+ GaAs layers, one of the diodes is forward biased and the other one is reverse biased depending on the bias polarity. The forward biased diode will only carry small reverse leakage current of the reverse biased voltage due to series connection of these diodes. Since this current is very low, voltage across the forward biased diode is very low and most of the applied bias drops across the reverse biased diode. Under high-speed operation, device is equivalent to two capacitors in series. Since the depletion width of the top *np* diode is thinner than the *i*-region of the bottom *pin* diode, capacitance of the top *np* diode is greater than that of the bottom *pin* diode. Hence, the effective capacitance is approximately equivalent to the capacitance of the bottom *pin* diode. Therefore, this design effectively works as a *pin* design.

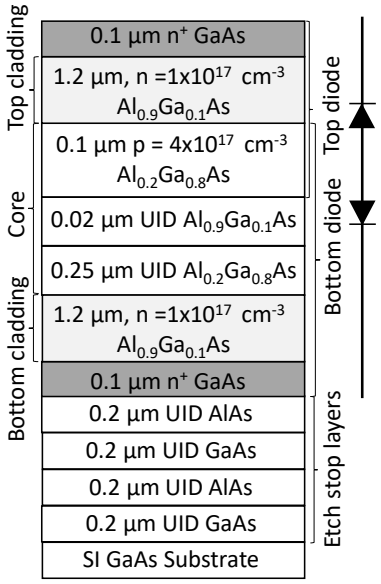

Fig. 1. Details of the epitaxial layers and their functions.

The epilayer contains a slab waveguide with mostly $Al_{0.2}Ga_{0.8}As$ core and $Al_{0.9}Ga_{0.1}As$ upper and lower claddings. The 1.2 μm thick *n* $Al_{0.9}Ga_{0.1}As$ bottom and the top claddings are sufficiently thick to reduce the optical mode overlap with the n^+ GaAs layers. n^+ GaAs is used for making low resistance alloyed ohmic contacts to the top and the bottom diodes. Doping in *p* and *n* regions were kept moderately low to reduce the propagation loss. Thin 0.02 μm UID $Al_{0.9}Ga_{0.1}As$ acts as the barrier to localize the holes in *p* $Al_{0.2}Ga_{0.8}As$.

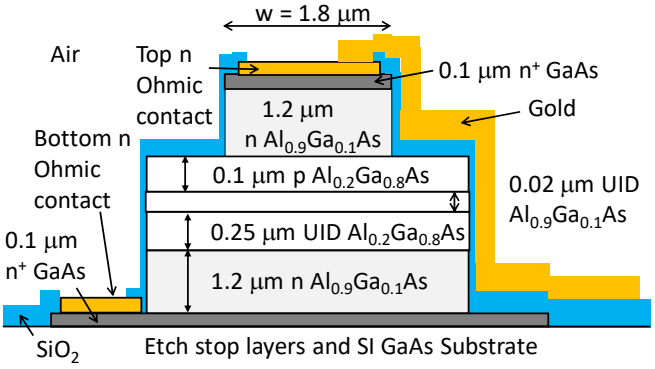

Fig. 2. Details of the optical waveguide used in the modulator.

The waveguide used in the modulator is shown in Fig. 2. It is designed to be a rib waveguide, which is 1.8 μm wide and 1.3 μm deep. 1.3 μm deep etch includes 0.1 μm n^+ GaAs and 1.2 μm *n* $Al_{0.9}Ga_{0.1}As$. Overlap of the optical mode with the etched sidewalls is minimal, which is crucial for low propagation loss. The mode shape fitted to a Gaussian has $1/e^2$ full width of approximately 0.72 μm in the vertical direction in the middle of the waveguide.

Doping in the bottom *n* $Al_{0.9}Ga_{0.1}As$ cladding ensures that,

the thickness of high electric field region due to an applied voltage is very close to the thickness of the *i*-region. This makes the gap of the electrode around 0.25 μm and results in efficient modulation. Optical mode field intensity is maximum in the *i*-region where the electric field due to applied voltage is also maximum ensuring a high overlap factor. Low electrode gap and high overlap factor combination results in low V_π.

This design can also deliver a device that can handle very high optical powers. At high optical powers, main issues are the facet damage and increased propagation loss. Facet damage can be dealt with by widening the waveguide and using special coatings. Increase in the propagation loss at high optical powers is mainly due to two-photon absorption, where two photons are absorbed simultaneously. Hence, strong absorption at and above half the material bandgap becomes possible. In the optical waveguide, the lowest bandgap energy belongs to $Al_{0.2}Ga_{0.8}As$, which is 1.673 eV. Bandgap of $Al_{0.9}Ga_{0.1}As$ is indirect and higher. This lowest bandgap energy is greater than twice the photon energy at 1.55 μm and significantly reduces two-photon absorption at high input powers making this device suitable for high power operation.

Fig. 3 shows the calculated energy band diagram of the device under different biases using a software package called Atlas from Silvaco [13].

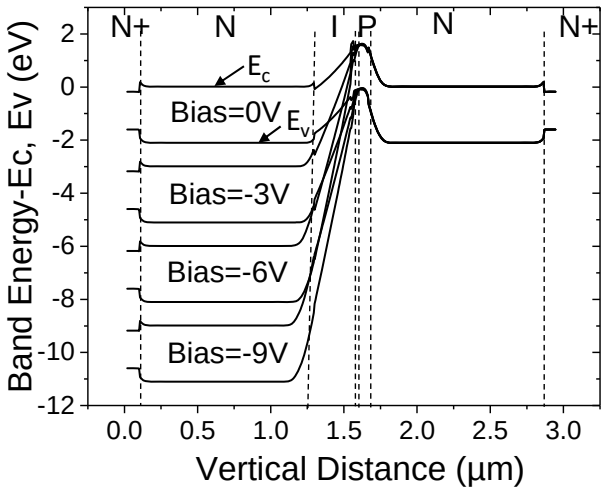

Fig. 3. Calculated energy band diagram of the device in the vertical direction at different applied biases. Surface is at the beginning of the rightmost n^+ layer.

Changes in the band diagram of the top *np* diode at all bias levels shown is negligible, which shows that the voltage drop across this diode is essentially zero. It is observed that the entire bias drops across the *i* layer for all biases. This creates a very high electric field across this region. As bias increases, both the bottom *n* $Al_{0.9}Ga_{0.1}As$ and *p* $Al_{0.2}Ga_{0.8}As$ layers starts to deplete and effective thickness of *i*-region increases slightly. Depletion induced decrease in hole concentration and overlap of the holes in the *p* layer reduces the free carrier absorption. However, even under 9 V bias there are sufficient holes to create a barrier at the order of the bandgap of $Al_{0.2}Ga_{0.8}As$ to suppress current flow between top and bottom n^+ GaAs layers. But, at a sufficiently high bias, *p* layer eventually depletes and current starts to flow between the top and bottom contacts. In the actual device, there is a low level of unintentional doping in the *i*-region. This layer eventually depletes under sufficiently high bias and the situation becomes very similar to what is shown in Fig. 3 at high biases. The desired mode of operation is a sufficiently high bias that depletes the *i*-region completely and most of the *p* layer, but current flow is still blocked. This sets up a very high electric field overlapping very well with the optical mode while keeping the free carrier absorption due to holes at a minimum. There will be additional propagation loss if the rest of the device such as y-branches and input and output sections are made out of the same waveguide. This loss could be kept low by depleting these sections using additional electrodes and keeping them short.

A numerical analysis is used to determine the V_π of the modulator. First Silvaco [13] is used to calculate the energy band profiles, electric field and carrier concentrations at different biases. The required mode profile is calculated using Beam Prop from Synopsis [14]. These computed parameters were combined in Matlab to calculate the overlap factors of the optical mode with the electric field, free carriers and depletion regions. This allows the calculation of phase change as the applied reverse bias is increased. The results of this calculation for an electrode length of 1 cm is shown in Fig. 4.

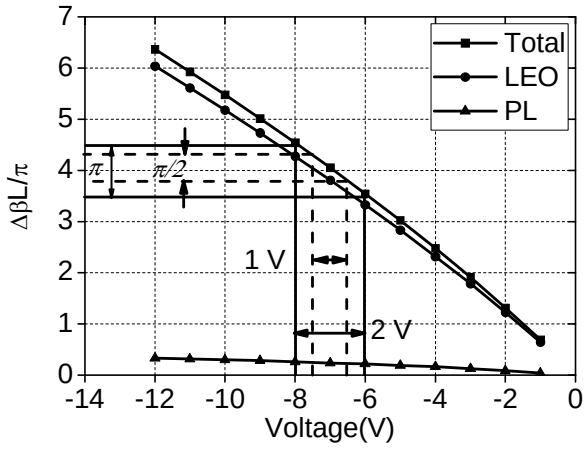

Fig. 4. Normalized phase change due to different physical effects as a function of applied voltage. Required voltages for π and $\pi/2$ phase changes at 7 V reverse bias are also indicated.

This figure shows contributions to the index change induced phase shifts due to linear electro optic (LEO) effect and the plasma effect (PL). In addition there could be a contribution due to quadratic electro-optic effect (QEO), but this contribution decreases exponentially with the bandgap and photon energy separation and in this design is negligible. Contribution from LEO effect is dominant. Depletion of charge in *p* and *n* regions contributes to PL effect. PL contribution to phase change is low due to low depletion and low overlap of depleted regions with the optical mode. The sign of LEO effect contribution depends on the waveguide alignment with respect to crystal axis. Waveguides were aligned along $[1\bar{1}0]$ for the index changes due to LEO and PL effects to add up. For a device biased at -7

V, phase change accumulated is 4π. V_π for single arm drive, which requires a π phase change, is 2 V at -7 V bias. For push pull drive, the phase change required in each arm is only π/2. This reduces the V_π to 1 V. A simple back of the envelop calculation using a formula where only LEO effect contribution to V_π is considered gives a similar result. This formula is $V_\pi = (\lambda t)/(2 r_{41} n_e^3 L \Gamma)$ and is for an electro-optic modulator operating under push pull drive. Here λ is the wavelength, t is thickness of i-region or electrode gap, r_{41} is the electro optic coefficient, n_e is the effective index of fundamental mode, L is the length of electrode and Γ is the overlap of the optical mode with i-region. With $\lambda = 1.55$ µm, $t = 0.27$ µm, $L = 1$ cm, $n_e = 3.1$, $r_{41} = 1.4$ pm/V and $\Gamma = 0.46$, V_π is 1.1 V. This result is close to the result of the complete simulation, which takes into account the small contribution due to PL effect.

III. PROCESSING DETAILS

Details of the fabrication process are illustrated in Fig. 5. Processing starts with the deposition and lift-off of metal stack consisting of Ni/Ge/Au/Ni/Au 5/18/132/20/300 nm to make alloyed ohmic contact to top n^+ GaAs.

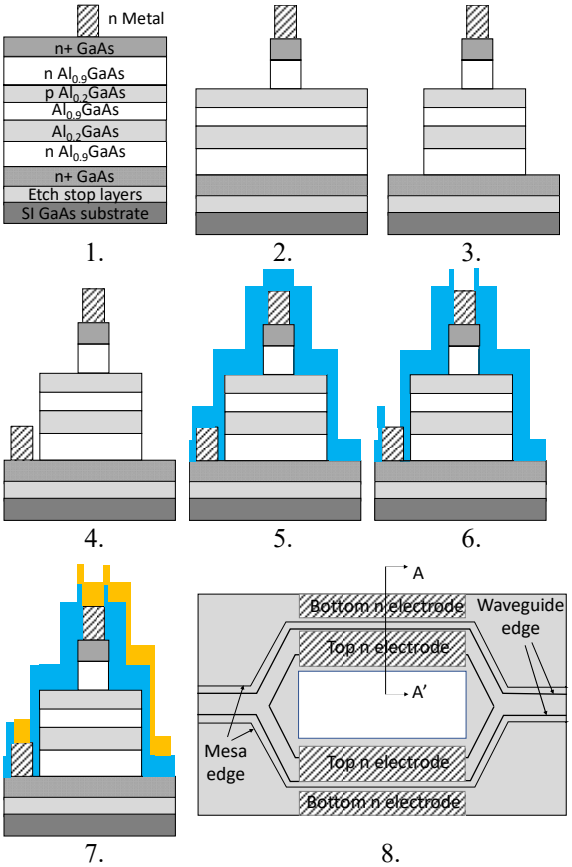

Fig. 5. Process steps used in the fabrication. 1. Top n^+ GaAs contact metal. 2. Waveguide etching. 3. Mesa etching. 4. Bottom n^+ GaAs contact metal. 5. Contact annealing and SiO_2 deposition. 6. Top and bottom contact openings. 7. Contact pad metallization. 8. Top schematic of the Mach-Zehnder modulator. Cross sectional profiles shown are at AA'.

After that, 0.25 µm thick PECVD oxide was deposited at 250ºC to be used as a hard mask for waveguide etching. After patterning the oxide using photoresist mask, 1.8 µm wide and 1.3 µm deep rib waveguide consisting of n^+ GaAs and n $Al_{0.9}Ga_{0.1}As$ are etched in Cl_2/N_2 chemistry using an ICP etcher. 10 µm wide mesas were then etched using a combination of dry and wet etching. In this step first, a photoresist - mask and ICP is used and etch was timed to stop on the bottom n $Al_{0.9}Ga_{0.1}As$. Then the sample was dipped in BHF for 10 seconds to etch the remaining n $Al_{0.9}Ga_{0.1}As$ and stop on bottom n^+ GaAs. Same metal stack used for top n^+ GaAs were lifted-off to make contacts to the bottom n^+ GaAs. At this point, both contacts were annealed at 430ºC in forming gas for 30 seconds. Next, 1.5 µm thick oxide was deposited using PECVD at 250ºC to reduce the overlap of the optical mode with the metal pads. Using a photoresist mask, metal contacts to top and bottom n^+ GaAs were reached by etching oxide in ICP. Finally, thick metal pads running on the waveguide sidewall and consisting of Ni/Au 50/1500 nm were lifted off to bring the top contact to the probing pads on the side of the device. Overall chip length was is 16 mm. Length of each y branch was 1.5 mm and electrode length varied to a maximum of 10 mm. Facets were not coated.

IV. RESULTS

For push pull operation, arms of the interferometer must be isolated to apply voltage to arms independently. This is naturally achieved due to high resistance of top n $Al_{0.9}Ga_{0.1}As$ cladding in narrow and long waveguides that join in the y-branch. Bottom n^+ GaAs is too heavily doped and wide to provide such isolation between the arms. So n layer of bottom pin diode was kept at ground potential during the measurements. The measured resistance between the top n contacts of the arms of a MZM is greater than 0.2 MΩ and limits the current flow between top n contacts to less than 100 µA. The current and capacitance as a function of voltage of a single arm of a MZM is shown in the Fig. 6. In this case, electrode is 1 cm long.

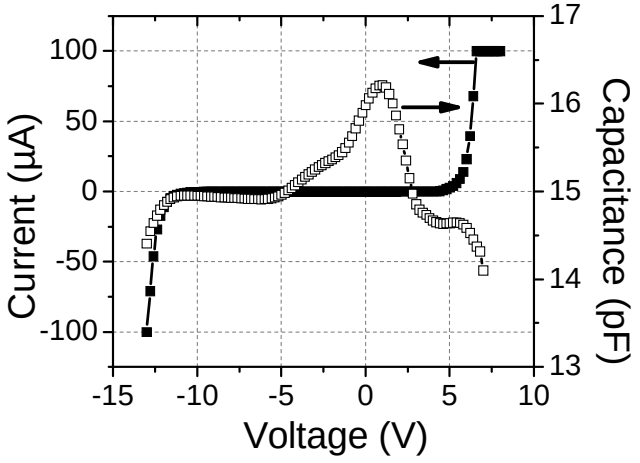

Fig. 6. Variation of the current and capacitance of a single arm of a MZM with 1 cm long electrode as a function of applied bias.

When bottom n contact is grounded and top n contact is positively biased, the top np diode is reverse biased. The bottom

pin diode is reverse biased when a negative bias is applied to the top *n* contact. In this case, there is negligible current flow until -12 V. After -12 V, *p* layer completely depletes making the device a resistor and current starts to flow between top and bottom *n* contacts. Along the positive sweep, this happens around 5.5 V since depletion layer of the *np* diode is thinner than the *i*-region of the *pin* diode. This makes the electric field higher and *p* layer depletes faster. Index changes due to charge injection and heating effects are ruled out as long as the device operation takes place in the voltage range where current is negligible.

Device capacitance starts higher and quickly reduces to a constant value as reverse bias to *pin* diode is increased. Capacitance initially does not flatten out because of the unintentional doping in the *i*-region. As the reverse bias is increased, charge in the *i*-region is depleted until eventually capacitance remains constant. When the *p* layer completely depletes, device is no longer a capacitance and the data loses its meaning. Decrease in the capacitance under bias is about 8%, which indicates very low unintentional doping. The desired voltage range for modulator operation is between 5 V to 10 V. In this range, there is a strong and constant electric field in the *i*-region, strong depletion of the *p* layer and constant device capacitance. Capacitance in this region is measured to be 1.88×10^{-16} F/μm^2 using large test structures. This means a 1.8 μm wide waveguide etched through the *p* layer will have about 3.5 pF/cm capacitance, which is suitable for high-speed operation. This is quite a bit different from the data shown in Fig. 6 since *p* layer is not completely removed outside the width of the waveguide and due to big contact pads.

Devices were cleaved at both ends and excited by a lensed fiber with a Gaussian output profile of 2.5 μm 1/e^2 full width at the input for optical testing. Output was collected and projected on an InGaAs photodetector using a 20x microscope objective lens. SEM picture of a cleaved facet is shown in Fig. 7. All the device layers and the thick SiO_2 layer are evident. In this case, the rib etch extended slightly into the *p* layer.

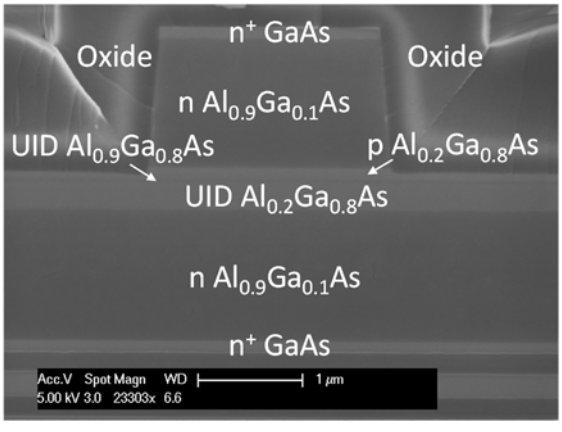

Fig. 7. SEM picture of a cleaved facet showing the cross sectional profile of a waveguide and device layers.

A sinusoidal modulating signal with a DC offset was applied to either a single arm or both arms of the device for measuring the optical response. Sinusoidal modulating signal with equal amplitude and opposite polarity was applied to both arms of the interferometer for push pull measurements. The DC bias applied to both arms was the same. Normalized transfer function of a MZM with 1 cm long electrode at 1.55 μm is shown in Fig. 8. V_π at -4 V bias is 2.16 V and 1.11 V under single arm and push pull drive respectively. Fig. 9 shows the normalized transmission of the same device at two other reverse biases under push pull drive. Increasing the reverse bias to 8 V results in $V_\pi = 1.01$ V which is about 10% less compared to V_π under 4 V reverse bias. V_π goes up to 1.3 V at 2 V reverse bias, which is about a 20% increase compared to 4 V reverse bias operation and a 30% increase compared to 8 V reverse bias operation.

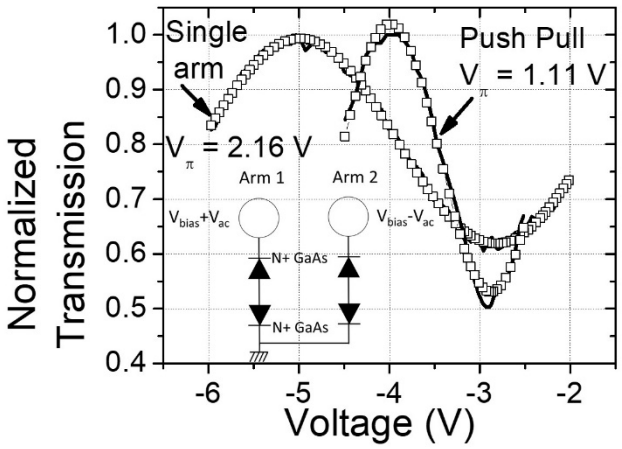

Fig. 8. Normalized transfer function of a modulator around -4 V bias under single arm and push pull drive at 1.55 μm. The modulator electrode is 1 cm long. The insert shows the equivalent circuit used for push pull drive.

This bias dependent V_π arises due to unintentional doping in the *i*-region. There is charge in the *i*-region as observed in the capacitance behavior, which reduces the electric field and its overlap with the optical mode. This increases V_π until all the charge is swept away. This happens after 5 V reverse bias. Change in V_π with bias voltage is negligible after this bias. Operation in this bias range is desirable since it not only gives the lowest V_π but also reduces the free carrier absorption due to depletion of holes in the *p* layer. On chip propagation loss at zero bias is estimated to be ~ 4-5 dB/cm based on Fabry-Perot measurements on phase modulators. This is also a conservative measurement since the fringe visibility is reduced due to stray light. A major contributor to this loss is found to be the metal running along the waveguide sidewall connecting the top contact to the contact pads. The propagation loss of waveguides on as grown material is measured to be 1.5 – 2 dB/cm. Hence, the additional loss due to metal is about 3 dB/cm. Extinction ratio is low and around 3 dB. The main limitation of the extinction ratio is due to the deep mesa etch around waveguides. This provides a wide high index region, which acts as a multi-mode waveguide. During the input excitation the modes of this mesa waveguide are inevitably excited and travel from the input

to the output. Even though they overlap with the applied electric field, they experience minimal modulation due to very large number of modes in this mesa waveguide. This provides at the output an unmodulated light level and decreases the extinction ratio and makes it somewhat coupling dependent. Furthermore, even under modulation, the higher order mode generated in the output waveguide after the *y*-branch leaks into and is trapped in this mesa waveguide. Some of this light is detected along with the modulated light in the output waveguide and reduces the extinction ratio. Appropriate mode transformers should eliminate this problem [15], [16].

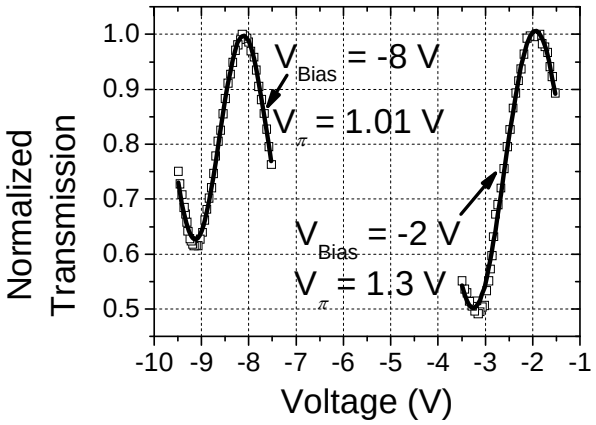

Fig. 9. Normalized transfer function of a modulator with 1 cm long electrode under push pull drive at 1.55 μm under two different bias voltages.

In order to investigate the optical power handling capability of the modulator a phase modulator optical transfer function and current voltage characteristics were measured at increasing optical input powers. The output of a 1.55 μm DFB laser was amplified using a high optical power fiber amplifier. The fraction of the input power that couples into the waveguide depends on the coupling loss. This loss has two components. One is the reflection from the facet and the other is the mode mismatch loss between the waveguide mode and the tapered fiber mode. Reflection loss is estimated to be around 1.3 dB per facet. Calculations using the overlap of the calculated fundamental mode of the rib waveguide and the mode profile of the lensed fiber, which is described earlier, yield the mode mismatch loss as 6.2 dB per facet. Therefore, total coupling loss per facet is around 7.5 dB. This means only about 18% of the optical power available from the source enters the waveguide. In the rest of the discussion, we quote the estimated coupled input power, $P_{\mathrm{Est}}^{\mathrm{In}}$. These power levels are a lower bound due to additional light entering and being trapped in the mesa and actually, there is more power in the entire epilayer. Fig. 10 shows a 5.5 mm phase modulator and its transfer function as a function of applied voltage when $P_{\mathrm{Est}}^{\mathrm{In}} = 35$ mW. In this case, output power of the modulator coupled to a detector is 3 mW. In this measurement, the lower *pin* diode is reverse biased.

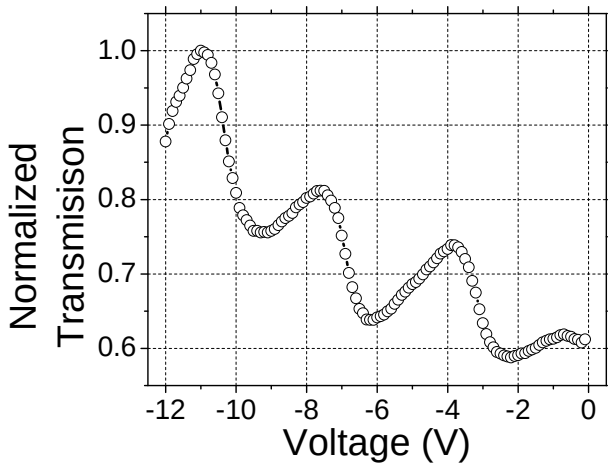

Fig. 10. Normalized transfer function of a 5.5 mm long phase modulator at 1.55 μm as a function of applied voltage when $P_{\mathrm{Est}}^{\mathrm{In}} = 35$ mW.

The transfer function of this phase modulator is as expected and the voltage span between two adjacent peaks corresponds to a π phase shift. Hence, this voltage is the same as V_π of a MZM under single arm drive. In this case $V_\pi = 3.78$ V which corresponds to a V_π length product of 2 V-cm under single arm and 1 V-cm under push pull drive. This is in agreement with the result presented in Fig. 9.

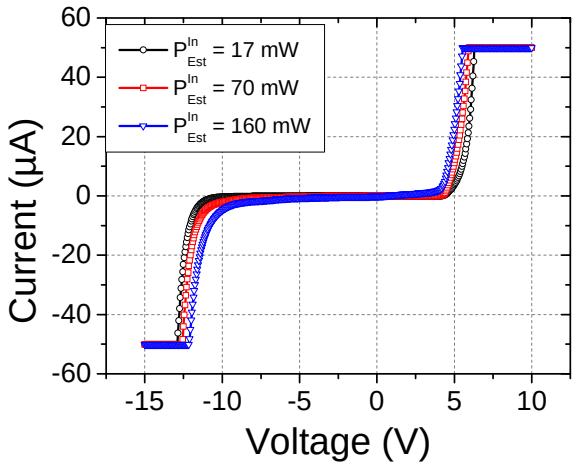

Fig. 11. Current as a function of voltage applied at different input power excitations for a 6 mm long phase modulator.

The current voltage characteristics of a 6 mm long phase modulator when input power is increased is shown in Fig. 11. There is some evidence of increased absorption as input power increases, especially when the electric field is the highest. This is most likely due to bandgap lowering due to Franz-Keldysh effect, which increases the absorption below bandgap at high electric fields. Increased absorption increases the device current due to photo detected current. This photo detected current is due to absorbed light in the entire mesa and waveguide, since *p* layer outside the waveguide is not etched and high electric field exists in the entire structure. However, even when $P_{\mathrm{Est}}^{\mathrm{In}} = 160$ mW,

increase of the current due to absorption in the desired operation region of less than 10 V bias is less than 5 μA. This indicates minimal absorption at high input optical powers demonstrating the suitability of the device for high optical power handling If the core of the waveguide were GaAs as opposed to $Al_{0.2}GaAs$ photo detected current due to two-photon absorption would be significantly higher. This current can be estimated using the two-photon absorption coefficient at a given optical power level, which is $\alpha_{\mathrm{TPA}} = \frac{1}{2}\Gamma\beta\frac{P}{A}$. In this expression Γ is the overlap of the optical power, *P*, in the waveguide with the absorbing material, β is the two-photon absorption coefficient for GaAs, *A* is the mode effective area [17]. Using typical values in our experiment, which are $\Gamma = 0.5$, $\beta = 24$ cm/GW [10], $P = 100$ mW, $A = 2\ \mu\mathrm{m} \times 3\ \mu\mathrm{m}$ we find $\alpha_{\mathrm{TPA}} = 0.01\ \mathrm{cm}^{-1}$. Under band-to-band absorption, the waveguide can be treated as a photo detector. The quantum efficiency of such a detector is $\eta = \eta_{\mathrm{int}}\left(1 - e^{-\alpha_{\mathrm{TPA}}L}\right)$, where *L* is the length of the waveguide or phase modulator. This calculation yields $\eta = 4.489\times10^{-3}$ for $L = 0.5$ cm and $\eta_{\mathrm{int}} = 0.9$. The corresponding responsivity is $R = \frac{\eta\lambda(\mu\mathrm{m})}{1.24} = 5.6\times10^{-3}$. Then the photo detected current that will appear under reverse bias would be $I_d = RP = 561$ μA This is at least two orders of magnitude higher than what we observe. Although this is not an exact calculation, it clearly shows that two-photon absorption is strongly suppressed and the design presented is suitable for high power operation. Measured values of two-photon absorption coefficient for waveguides with $Al_{0.18}GaAs$ cores are around 0.25 cm/GW, which further support this conclusion [18]

V. CONCLUSION

Bulk AlGaAs electro-optic Mach-Zehnder intensity modulators are reported. Modulator uses an *npin* design, which is effectively equivalent to a *pin* design. *nipn* design eliminates high resistance *p* ohmic contacts. Modulator design, simulation and fabrication have been described. Fabrication requires conventional processing, which can take advantage of professional foundry processes. Measurements indicate current through the device is minimal under reverse biases approaching 12 V. There is some bias dependence of the modulator capacitance due to unintentional doping in the *i*-region. Once this charge is depleted modulator capacitance remains constant over a wide voltage range. This capacitance is low enough to enable wide bandwidth traveling wave designs based on loaded line approach. Modulators with 1 cm long electrodes have 1 V V_π. Some bias dependence of V_π due to unintentional doping in the *i*-region is also observed. Once this charge is depleted, the modulator characteristics remain stable. The lowest bandgap in the device is larger than twice the photon energy at 1.55 μm. This significantly reduces material absorption including two-photon absorption. Modulator performance remains unchanged under coupled input optical powers approaching 160 mW. Combined with low V_π makes these modulators suitable for analog photonic link applications.

REFERENCES

[1] C. H. Cox, "Analog Optical Links, Theory and Practice", Cambridge University Press, ISBN 9780521027786, 2006.

[2] N. Dagli," Wide Bandwidth Lasers and Modulators for RF Photonics," IEEE Trans. Microwave Theory Tech., vol. MTT-47, No. 7, pp. 1151-1171, July 1999.

[3] N. Dagli, "Optical Modulators", Handbook of Optoelectronics, 2nd Edition: Concepts, Devices and Techniques, vol. 1, Chapter 14, pp. 457-514, CRC Press, Taylor and Francis, 2018.

[4] W. M. J. Green, M. J. Rooks, L. Sekaric, and Y. A. Vlasov, "Ultra-compact, low RF power, 10 Gb/s silicon Mach-Zehnder modulator "Optics Express, vol. 15, No.25, pp. 17106, Dec. 10, 2007.

[5] X. Zhang, A. Hosseini, S. Chakravarty, J. Luo, A. K.-Y. Jen and R. Chen, "Wide optical spectrum range, subvolt, compact modulator based on an electro-optic polymer refilled silicon slot photonic crystal waveguide "Optics Letters, vol. 38, No. 22, pp. 4931-4934, 15 November 2013.

[6] J. Liu, G. Xu,F. Liu, I. Kityk, X. Liu, Z. Zhen, "Recent advances in polymer electro-optic modulators", Royal Society of Chemistry Advances, vol. 00, pp. 1-3, 2014, DOI: 10.1039/x0xx00000x.

[7] S. Dogru and N. Dagli, "0.2 V Drive Voltage Substrate Removed Electro-Optic Mach-Zehnder Modulators with MQW cores at 1.55 μm," IEEE/OSA J. of Lightwave Technology, vol. LT-32, No. 3, pp. 435-439, February 1, 2014.

[8] S. Dogru and N. Dagli, "0.77-V drive voltage electro-optic modulator with bandwidth exceeding 67 GHz", Optics Letters, vol. 39, No. 20, pp. 6074-6077, 15 October 2014.

[9] A. Villeneuve, C. C. Yang, G. I. Stegeman, C. N. Ironside, G. Scelsi, and R. M. Osgood, "Nonlinear absorption in a GaAs waveguide just above half the band gap," IEEE J. Quantum Electron., vol. 30, no. 5, pp. 1172–1175, May 1994.

[10] J. H. Shin and N. Dagli, "Ultra-low drive voltage substrate removed GaAs/AlGaAs electro-optic modulators at 1550 nm" IEEE Journal of Selected Topics in Quantum Electronics, Special Issue on Modulators, vol. 19, No. 6, pp. 3400408, Nov-Dec 2013.

[11] J. H. Shin, C. Ozturk, S. R. Sakamoto, Y. J. Chiu and N. Dagli, "Novel T-Rail Electrodes for Substrate Removed Low-Voltage, High-Speed GaAs/AlGaAs Electro-optic Modulators, " IEEE Trans. Microwave Theory Tech. vol. MTT-53, No. 2, pp. 636 – 643, February 2005.

[12] P. Bhasker, J. Norman, J. Bowers, and N. Dagli, "Low Voltage, High Optical Power Handling, Bulk GaAs/AlGaAs Electro-optic Modulators", Integrated Photonics Research, Silicon, and Nano-Photonics Conference proceedings, paper IW3B.4, Zurich, Switzerland, 2-5 July 2018.

[13]https://www.silvaco.com/products/tcad/device_simulation/atlas/atlas.html

[14] https://www.synopsys.com/optical-solutions/rsoft/passive-device-beamprop.html

[15] Selim Dogru and Nadir Dagli. "Mode Transformers for Substrate Removed Waveguides", Proceedings of IEEE Photonics Society Annual Meeting (IEEE Photonics 2013), paper MF1.3, pp. 102-103, Bellevue, Washington, 8-12 September 2013.

[16] P. Bhasker, S. Dogru and N. Dagli, "Active-Passive Integration using a-Si waveguides for Substrate Removed Electro-Optic Modulators, "2018 IEEE Photonics Conference (IPC), DOI: 10.1109/IPCon.2018.8527092, Reston, VA, 30 September-4 October 2018.

[17] D. Duchesne, L. Razzari, L. Halloran, R. Morandotti, A. J. SpringThorpe, D. N. Christodoulides, and D. J. Moss, "Two-photon photodetector in a multiquantum well GaAs laser structure at 1.55μm, " Optics Express, vol. 17, No. 7, pp. 5298- 5310, 30 March 2009.

[18] Alain Villeneuve, C. C. Yang, George I. Stegeman, Chen-Hui Lin, and Hao-Hsiung Lin, "Nonlinear refractive-index and two photon-absorption near half the band gap in AlGaAs, Appl. Phys. Lett. Vol. 62, pp. 2465, 1993.

Prashanth Bhasker received his B.E degree from Anna University in India. Currently he is working towards his Ph.D. in the Electrical and Computer Engineering Department of University of California at Santa Barbara. His interests are design, fabrication and testing of advanced photonic components. He is a member of IEEE.

Justin Norman received B.S. degrees in Physics and Chemical Engineering from the University of Arkansas, Fayetteville in 2013. He is currently pursuing a Ph.D. in Materials at the University of California, Santa Barbara as an NSF and Frenkel Foundation Fellow. His research interests include molecular beam epitaxial growth of InAs quantum dot lasers on silicon, direct III-V growth on Si, and quantum dot microcavities for cavity quantum electrodynamics.

John Bowers (F'94) is Director of the Institute for Energy Efficiency and a distinguished professor in the Departments of Electrical and Computer Engineering and Materials at the University of California, Santa Barbara. His research interests are primarily concerned with silicon photonics, optoelectronic devices, optical switching and transparent optical networks and quantum dot lasers. Bowers received the M.S. and Ph.D. degrees from Stanford University. He worked for AT&T Bell Laboratories and Honeywell before joining UCSB. Bowers is a fellow of the IEEE, OSA and the American Physical Society, and a recipient of the IEEE Photonics Award, OSA/IEEE Tyndall Award, the IEEE LEOS William Streifer Award and the South Coast Business and Technology Entrepreneur of the Year Award. He is a member of the National Academy of Engineering and the National Academy of Inventors.

Nadir Dagli (F'06) received the Ph.D. degree in electrical engineering from MIT in 1986. After graduation he joined the electrical and computer engineering department at University of California at Santa Barbara, where he is currently a Professor and Chairman. His current interests are design, fabrication and modeling of guided-wave components for optical integrated circuits, ultrafast electro-optic modulators, WDM components and photonic nanostructures. He served and chaired many conferences, technical program and other professional committees. He was the Editor-in-Chief of IEEE Photonics Technology Letters 2000-2005 and an elected member of the IEEE-LEOS board of governors 2003-2005. He is a Fellow of IEEE and OSA.